Mitigating blade erosion damage through nowcast-driven erosion-safe mode control

Barfknecht, N.; Imhoff, R.; Von Terzi, D.

Important note
To cite this publication, please use the final published version (if applicable).
Please check the document version above.

PAPER • OPEN ACCESS

Mitigating blade erosion damage through nowcast-driven erosion-safe mode control

View the article online for updates and enhancements.

Mitigating blade erosion damage through nowcast-driven erosion-safe mode control

N Barfknecht[1], R Imhoff[2], D von Terzi[1]

[1]Delft University of Technology, Faculty of Aerospace Engineering, Wind Energy Group, Kluyverweg 1, Delft, The Netherlands
[2]Deltares, Operational Water Management & Early Warning, Boussinesqweg 1, Delft, The Netherlands

E-mail: `n.barfknecht@tudelft.nl`

Abstract. The erosion-safe mode (ESM) is a novel mitigation strategy that reduces rainfall-induced erosion damage by lowering the tip-speed of the turbine during precipitation events. The ESM requires accurate information about future expected rainfall for its control. In current research, it is debated what method or source should be used to this end. This study explores the effectiveness of driving the ESM using a state-of-the-art weather-radar-based probabilistic rainfall nowcast provided by the Royal Netherlands Meteorological Institute (KNMI). The performance of the nowcast is assessed for various lead times with an impingement-based damage model for three sample sites in the Netherlands and for two distinct ESM strategies. The results show that the quality of the nowcast degrades with increasing lead times, where the 5- and 15-minute lead times exhibit sufficiently good accuracy and response time for adjusting turbine speeds. Overall, the results highlight that the probabilistic information in the nowcast can be employed to improve the efficiency and viability of the ESM.

1. Introduction

Leading-edge erosion is a severe problem for the wind energy community. Hydrometeors impact the wind turbine's blade during precipitation events, leading to structural damage and roughening of the blades. The latter leads to a reduction in the annual energy production (AEP) in the order of several percent. Current mitigation strategies include the application of tapes and shields fitted to the leading edge of the blade. A novel mitigation method is the so-called erosion-safe mode (ESM) [1, 2], which aims to avoid erosion damage by reducing the tip-speed of the wind turbine during precipitation events. A reduction in tip-speed will also lead to a performance loss. Nevertheless, studies have shown that this strategy can lead to a lower AEP loss than an eroded blade [2]. The inherent performance loss of an ESM can be minimized if the ESM were to be only activated when damaging rain occurs. For this purpose, an accurate short-term forecast, ideally in the order of minutes to hours, is required. This time frame is currently covered by state-of-the-art meteorological nowcasting products, where radar-based observations are extrapolated in time using a variety of statistical and advection-based methods [3].

Tilg et al. [4] argue that several challenges exist with classical radar-based precipitation forecasts for offshore applications, such as radar clutter caused by wind farms. They, therefore, propose using a micro-rain-radar placed in the vicinity of a turbine to collect the required data. However, this necessitates extra hardware, which needs to be operated and maintained, and

it requires the construction of a well-performing rainfall product out of the radar reflectivity measurements. This adds complexity and cost, which is not always feasible. Therefore, it seems beneficial if, ideally, standard *off-the-shelf* forecasting products could be used to drive the ESM. An advantage of the Netherlands is that one of the C-band weather radars is located at the coast in the vicinity of the largest offshore wind farms, see Figure 1. Together with a recent reduction in clutter in the Dutch radar composite [5], this lowers the systematic errors in the radar product, as mentioned by Tilg et al. [4].

The objective of the present study is to investigate whether a state-of-the-art weather-radar-based precipitation nowcast product can be used to effectively drive the erosion-safe mode. To this end, the performance of the ESM is compared for being driven by the nowcast with being driven by rainfall measurements.

2. Methodology

2.1. Forecast products

Two weather-radar-based products are used. One serves as the ground truth of *true rain*. The other represents the nowcast used to determine the speed at which the wind turbine should operate.

rad_nl25_rac_mfbs_5min: The true rain was obtained from KNMI's rad_nl25_rac_mfbs_5min product [6]. It is a rain-gauge-corrected quality-controlled radar-based dataset that provides precipitation accumulations for the land area of the Netherlands on a grid with a 1x1 km resolution. This dataset is not available in real time, but it is generally considered a high-quality data set that can be used for reference purposes [7].

precipitation_NL_ensemble_nowcast_5min: For the forecast, KNMI's new state-of-the-art precipitation_NL_ensemble_nowcast_5min product was chosen [8]. The product is based on the open-source pySTEPS package, representing a probabilistic forecast of 20 ensembles [8, 7, 9]. It provides rainfall nowcasts in 5-minute increments up to 120 minutes in advance with a spatial resolution of 1x1 km. Its fine resolution provides the potential to control every turbine in a wind park individually based on the expected rainfall. Due to its novelty, the product data series has only a span of about ten months, running from 04:45 04/07/2022 to 01:55 07/05/2023 (time format: hh:mm DD/MM/YYYY). This range includes 77916 forecasts that were analyzed in this study. This product is termed *the nowcast* in the following.

The domain of both products is shown in Figure 1. It can be seen that the products span the entirety of the landmass of the Netherlands and, importantly, also the parts of the Dutch North Sea that are being developed for offshore wind parks.

For the purpose of this study, one important assumption with regard to the weather products was made. Both products indicate the rain at an altitude of 1500 m. As calculated in Tilg et al. [4], droplets require about 5 minutes to reach the ground from such altitude. Here, it is assumed that this time delay does not exist.

2.2. Wind turbine and sample sites

A model turbine is required for the evaluation of the ESM. For this purpose, the IEA 15MW reference wind turbine (RWT) was chosen since it represents the current generation of large offshore wind turbines [11]. Three sample sites are chosen for this investigation: The KNMI stations of De Kooy (#235), Herwijnen (#356) and Maastricht (#380). The number in parenthesis provides the KNMI station identifier. The De Kooy station represents a coastal site. The Maastricht station lies far inland in the Dutch province of Limburg. The Herwijnen station can be seen as an *in-between* station. The location of all three stations is shown in Figure 1.

For the official KNMI stations, wind data are provided as an hourly mean at a height of ten meters. It is assumed that the wind stays constant in the given hourly interval. The wind
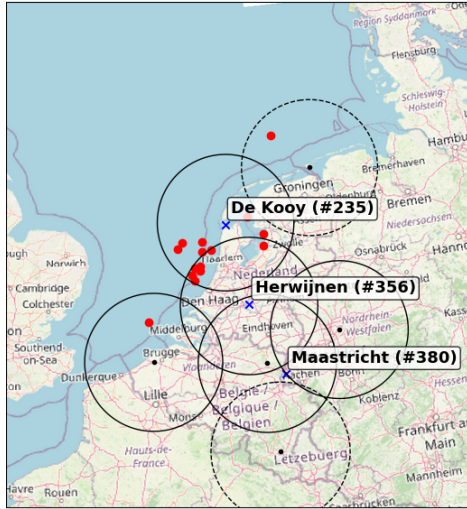
Figure 1: The figure shows the entire coverage area of the nowcast plotted in a stereographic projection; height of 765 km; width of 700 km; the three sample sites are indicated with a blue cross; current Dutch offshore wind farms are indicated with a red dot; the 100 km radius around weather radars is indicated by a solid black circle, outside this range a radar-based product usually degrades [10]; the dashed circles represent the German Borkum and Belgian Wideumont radars that are since recently used in some KNMI products; the background map is taken from OpenStreetMap released under the ODbL license.

speed at the IEA RWT's 150 m hub height is obtained by scaling the measured wind speed so that the mean wind speed coincides with the data provided by the Dutch Offshore Wind Atlas (DOWA) for 150 m height [12]. It was found that using a power law correction, as, for example, suggested by Verma et al. [13], yields a mean wind speed that greatly differs from the ones given by the DOWA. DOWA's data are deemed more reliable. The scaling coefficients applied to the 10 m wind measurements are 1.7742 (De Kooy, #235), 2.0157 (Herwijnen, #356) and 1.9386 (Maastricht, #380).

The IEA 15MW RWT is designed for a mean wind speed at hub height of 10 m/s [11]. However, the chosen sites have mean wind speeds of 9.2 (#235), 7.65 (#356) and 7.42 m/s (#380). Hence, the operational time at rated power is reduced. For a 10 m/s site the turbine would operate 42 % of the time at rated capacity. For the three sites, this becomes 35 (#235), 22 (#356) and 21 % (#380).

2.3. ESM strategy

The ESM exploits two characteristics of leading edge erosion. Firstly, the damage production is very sensitive to changes in the speed of the blade, and, secondly, erosion damage production increases as rain intensity increases [14]. In this study, two distinct ESM strategies are considered: the V-ESM and the VI-ESM. The V-ESM limits the tip-speed during precipitation events based on wind speed (V_{wind}). The VI-ESM limits the tip-speed based on wind speed and rain intensity (I). These strategies were developed in Barfknecht et al. [14], where it was shown that they are optimal strategies. They provide the highest damage reduction for the lowest possible AEP loss.

The ESM strategies can be defined by relations of the form

$$\text{V-ESM} = g_{\text{opt}}(V_{\text{wind}}), \qquad\qquad \text{VI-ESM} = g_{\text{opt}}(V_{\text{wind}}, I_{\text{nowcast}}), \qquad (1)$$

where g is a function relating environmental inputs, such as V_{wind} and I, to the turbine's tip-speed V_{tip}. g_{opt} is defined (for the VI-ESM) as

$$g_{\text{opt}} = \{g(V_{\text{wind}}, I) \quad \text{subject to} \quad \text{minimize}(|\eta(g(V_{\text{wind}}, I)) - K|) \quad \text{for all} \quad (V_{\text{wind}}, I)\}, \quad (2)$$

where

$$\eta(g(V_{\text{wind}}, I)) = \frac{\frac{\partial P}{\partial V_{\text{tip}}}}{\frac{\partial(\partial_t D)}{\partial V_{\text{tip}}}} = \frac{\partial P}{\partial(\partial_t D)}, \qquad (3)$$

and

$$g(V_{\text{wind}}, I) = \{g_{\text{min}}(V_{\text{wind}}) \leq V_{\text{tip}} \leq g_{\text{normal}}(V_{\text{wind}}) \text{ for all } (V_{\text{wind}}, I)\} . \tag{4}$$

P is the power of the turbine and $\partial_t D$ is the erosion damage production rate. Here, the probabilistic (continuous) formulation of the power and damage production for a particular site must be used, as explained in Barfknecht et al. [14]. g_{min} is the turbine's minimum speed. g_{normal} represents the turbine's normal tip-speed as a function of wind speed. In the method, a constant K is chosen. Subsequently, the tip-speed for every environmental input is chosen such that $\eta = K$, or when this is not possible, the η closest to K is selected. The resulting tip-speed for every V_{wind} and I is g_{opt}. η measures which tip-speeds as a function of V_{wind} and I add the most power for the lowest damage increase. A value of K leads to a particular tuple of AEP loss and damage reduction. By varying K, other tuples can be realized. The reader is referred to the original reference for the full description of the method and key assumptions in the derivation.

2.4. Calculation of damage and power

The damage model is based on impingement H, a metric for the accumulated water column by the blade. The damage model was developed in Barfknecht et al. [14] and incorporates several drop-size-dependent effects, such as the slowdown effect from Barfknecht et al. [15] and a drop-size-dependent damage law from Bech et al. [16]. Since the wind speed and the precipitation forecast are given as a discrete data set, the hybrid continuous-discrete approach from Barfknecht et al. [14] is used. It reads

$$D = \sum_{i=1}^{N} \left(\int_{0°}^{360°} \int_{0}^{\infty} \frac{\partial_t H(I_{\text{true rain}}(t_i), V_{\text{wind}}(t_i), \theta, \phi)}{H_{\text{allowed}}(V_{\text{wind}}(t_i), \phi)} f_{\phi,\text{plane}} f_\theta \, d\phi d\theta \right)_i \Delta T_i. \tag{5}$$

N is the number of elements in the data series. $f_{\phi,\text{plane}}$ is the drop size (ϕ) distribution through a plane, and f_θ is the uniform distribution of the blade position (θ). $\partial_t H$ is the impingement accumulation rate and H_{allowed} is the impingement until the end of the incubation time. V_{impact} is the impact speed of the droplets and is dependent on V_{tip}, V_{wind} and others. In this formulation the variables θ and ϕ are considered distributed and the variables I and V_{wind} are considered discrete. $\Delta T_i = t_i - t_{i-1}$ is the time step of a particular data frame i with time stamp t_i. For the products used in this study, ΔT_i is five minutes.

The power is calculated as $P = Q\omega$ with

$$C_Q(\lambda) = \begin{cases} M(\lambda) & \text{if } M(\lambda) < \left(C_{Q_{\text{max}}} = \frac{Q_{\text{max}}}{qAR} \right), \\ (C_Q(\lambda, \varphi_{\text{pitch}}) = C_{Q_{\text{max}}}) & \text{if } M(\lambda) \geq C_{Q_{\text{max}}}, \end{cases} \tag{6}$$

where $Q = q\,A\,R\,C_Q$ and $\omega = V_{\text{tip}}/R$. $M(\lambda) = \max(C_Q(\lambda, \varphi_{\text{pitch}}))$, ω is the rotational speed, q is the dynamic pressure, A is the rotor disk area, R is the rotor radius and C_Q is the torque coefficient. For any tip-speed ratio λ, the pitch angle φ_{pitch} is chosen such that the torque coefficient is maximized in the partial load region and limited to the rated generator torque Q_{max} in the rated power region. It is assumed that neither the blade position nor the droplet diameter influence the energy production. Hence, the produced energy becomes:

$$E = \sum_{i}^{N} P_i \Delta T_i. \tag{7}$$

Due to these assumptions, the equation becomes a simple summation over all the time steps. The reader should note that the definitions of P and D given in this section are different to those in Equation 3. The reader is referred to the original reference for an in-depth explanation.
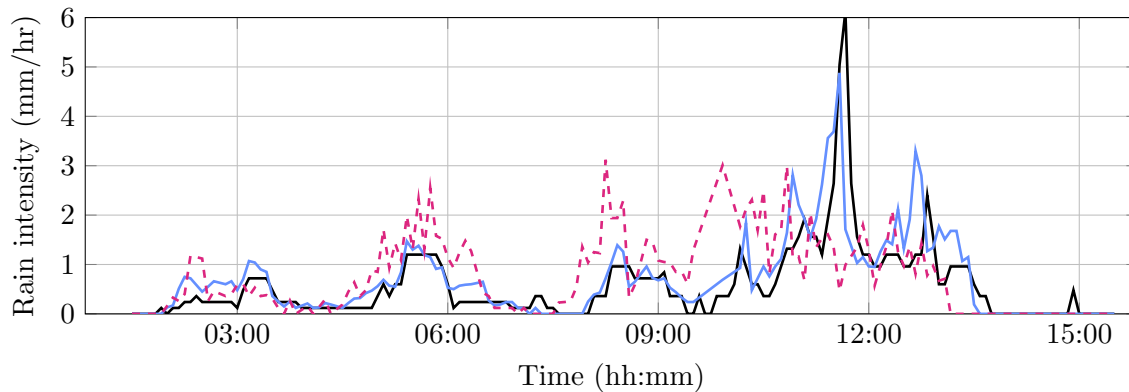
Figure 2: Actual rainfall observations and nowcasts for 21-07-2022 between 1:30 and 15:30 at station De Kooy. True rain (radar-corrected): ——, 15-min nowcast (1 ensemble): ——, 60-min nowcast (1 ensemble): - - -.

3. Results

The accuracy of the nowcasting product is essential for a successful utilization in the ESM. When the nowcast and the true rain do not correlate well, false-positive and false-negative control decisions are produced. As a consequence, the turbine will operate at reduced performance in dry conditions or will accumulate significant amounts of damage during precipitation events. Figure 2 provides an initial assessment of the performance of the nowcasting product at the 1x1 km grid cell above the site De Kooy. A rainfall event is shown that occurred in July 2022, when a low pressure area moved over central Netherlands, resulting in widespread rainfall with local convective activity. For this event, the true rainfall, based on the corrected radar product and the rainfall nowcasts for 15 and 60 minutes ahead, is given. The 15-minute nowcast performs well. It can accurately predict the rain intensity as well as the start and end times of the individual precipitation events. A deterioration in performance can be observed for the 60-minute nowcast, especially later during that day, which coincides with heavier rainfall intensities as a result of convective activity. Convective rainfall (thunderstorm) is more challenging to capture far in advance with nowcasting methods. New storms generally form within time spans of 30 minutes and thus cannot yet be part of the observations in the 60-minute nowcast [7].

3.1. Evaluation of single-ensemble nowcast

The accuracy of the nowcast is first assessed by considering a single (random) ensemble member. The total damage and energy is calculated for both series of the true rain and the nowcast. By considering a complete sweep of ESM coefficients K, see Equation 2, a Pareto front is spanned that shows the maximum attainable lifetime extension (LX = $L_{\text{ESM}}/L_{\text{no ESM}}$, L is the erosion incubation time) for a particular AEP penalty. The best possible Pareto front is obtained when the ESM is controlled with a perfect forecast, i.e., the ground truth rain is used. The goal of any nowcasting-controlled ESM is to approach this front as closely as possible. The nowcast is evaluated at lead times of 0, 5, 15, 30, 60 and 120 minutes. The V-ESM and VI-ESM strategies are considered. The results are shown in Figure 3.

Comparing the true rain Pareto fronts of the V-ESM and the VI-ESM shows that the latter performs significantly better. The start and end points of the respective V-ESM and VI-ESM Pareto (——) fronts are equal. The start (1, 0 %) represents an ESM strategy that never slows down the turbine, and the end point indicates a strategy that always slows down the turbine to minimum speed when rain is predicted. Between the start and end points, the considered ESM strategies can perform differently. Barfknecht et al. [14] obtained the same results but for
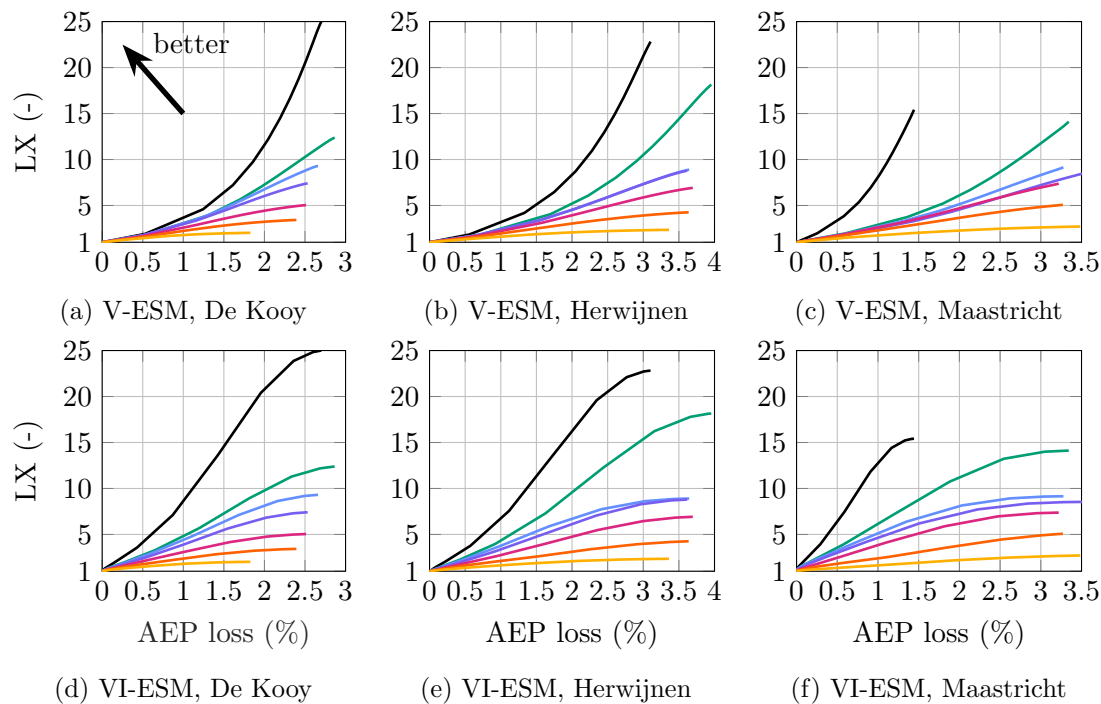
Figure 3: Single-ensemble results (Lifetime extension factor versus AEP loss) for the V-ESM and VI-ESM; three different sites were considered; Pareto front with perfect ground truth precipitation data: ——; Curves obtained using nowcast of 0-min: ——, 5-min: ——, 15-min: ——, 30-min: ——, 60-min: ——, 120-min: ——.

a completely probabilistic setting. For Herwijnen, the V-ESM can provide an LX of three for a 1 % AEP penalty. Whereas the VI-ESM strategy provides for the same AEP loss an LX of seven.

A comparison of the Pareto fronts across the three considered sites shows a reduction in maximum attainable LX when moving inland. This is caused by the reduced mean wind speed that causes the turbine to spin more frequently at minimum rotational speed. Hence, during (some) precipitation events, the turbine speed cannot be reduced further. However, it should also be noted that for lower mean wind speed, the absolute accumulated damage, even in the absence of the ESM, is reduced. It is also visible that moving inland increases the maximum AEP loss. Interestingly, the maximum LX for the 5 to 120-minute nowcasts is surprisingly similar across all sites, whereas pronounced differences exist for the 0-minute nowcast.

The curves of the nowcasts approach the Pareto front as the lead times are reduced, which is expected given the increasing quality of the nowcasts for shorter lead times [3, 7]. The 0-minute nowcast represents the current rain conditions. Ideally, it would perform similarly to the ground truth product. This is not the case due to the absence of quality-controlled rain gauge corrections in the operational radar product used in the nowcast, while such corrections are present in the ground truth reference product. Hence, a considerable gap exists between the ground truth Pareto front and the curve of the 0-minute nowcast. Nevertheless, the 0-minute nowcast can still achieve an LX of about five for a roughly 1 % AEP loss when the VI-ESM is used. The 5 and 15-minute nowcasts are generally close together and sometimes even overlap, as is the case for the Herwijnen station. The 30-minute nowcasts already show a considerable degradation in the performance. The 60 and 120-minute nowcasts perform poorly. For example, the 120-minute nowcasts can only achieve an LX of about two. This is an expected result, as it

has been found in the literature that the maximum skillfulness for a nowcast is limited to around 120 minutes [7]. From the results, it appears to be realistic to make ESM control decisions up to 15 minutes in advance.

Table 1 gives the values of the contingency table metrics for KNMI's De Kooy station for different nowcast lead times and months. The nowcasts have some gaps in the analyzed time span. Therefore, the data completeness (DC) is given. The 0 to 15-minute nowcasts retain good performance with hit rates (HR) above 79 %. The performance drops starting from the 30-minute nowcast due to increasing false negative (FN) values. The false positive (FP) values stay fairly constant across all lead times. Hence, the degradation of the nowcast performance can be attributed to the increase in FN as the lead times increase. This is shown in Figure 3. High FN values are associated with missed rain events. As the lead times increase, the AEP loss is reduced since the turbine fails to slow down due to missed events. This is accompanied by a reduction in the maximum LX. The table also shows that the single-ensemble nowcasts underestimate the total precipitation column. Note that the rain column reference values slightly differ due to the gaps in the dataset and the way the values are stored in the separate files that the KNMI provides.

Table 1: Contingency table for the De Kooy (#235) station; nowcast data are given for the entire period from 04/07/2022 until 07/05/2023 (DD/MM/YYYY); monthly values are given for the 15-minute nowcast; for the analysis by month note that the data length of July is slightly reduced due to the start date; the month of May was omitted since only 7 days of data were available; false positive (FP), false negative (FN), true positive (TP), true negative (TN), hit rate (HR), false positive rate (FPR), rain column (H), data completeness (DC). All data except H are given in %. H is given in mm.

Nowcast	FP	FN	TP	TN	HR	FPR	H_{now}	H_{true}	DC
perfect	0.00	0.00	7.50	92.50	100.00	0.00	727	727	100.0
0-min	1.43	0.88	6.62	91.07	88.23	1.55	519	631	88.2
5-min	1.32	1.21	6.27	91.20	83.85	1.42	509	629	88.2
15-min	1.41	1.56	5.92	91.11	79.15	1.52	455	628	88.2
30-min	1.70	2.11	5.38	90.81	71.82	1.83	479	627	88.2
60-min	2.17	3.03	4.45	90.35	59.51	2.35	365	633	88.2
120-min	2.00	4.53	2.99	90.48	39.78	2.16	204	624	88.2
July '22	0.37	0.56	2.53	96.54	81.90	0.39	16	17	93.0
August	0.22	0.32	1.57	97.89	83.13	0.23	50	41	94.6
September	2.81	2.01	8.68	86.50	81.24	3.14	90	113	91.2
October	0.98	0.86	2.72	95.44	75.97	1.01	17	33	96.5
November	2.47	2.53	11.73	83.27	82.24	2.88	98	155	89.1
December	1.51	2.18	5.40	90.91	71.27	1.63	36	55	92.0
January '23	2.24	2.06	8.35	87.35	80.20	2.50	42	64	74.4
February	0.55	1.17	2.18	96.10	65.13	0.57	4	13	72.2
March	2.36	2.80	10.41	84.43	78.80	2.71	52	78	83.2
April	0.82	1.42	6.18	91.58	81.29	0.88	47	57	99.2

The second part of the table analyzes the 15-minute nowcast values by month. A relatively constant hit rate can be observed with exceptions being the months of December 2022 and February 2023. However, during the latter hardly any precipitation occurred and only 4 out of 13 mm of rainfall was forecasted. In the tested period, there was more rain in the winter than in the summer months and also the probability of having rain was higher during winter. It is

noteworthy that the summer months of 2022 were unusually dry in the Netherlands and usually the precipitation column is rather constant across the months. During these months the TP rate is increased since more rain events are correctly forecasted. However, also the FP and FN rates are increased, which is caused by the higher number of precipitation events in winter.

3.2. Evaluation of multiple-ensemble nowcast

The nowcast contains 20 ensembles, i.e., for every lead time, the nowcast predicts 20 possible outcomes. It, therefore, contains probabilistic information, capturing the uncertainty in the rainfall forecast. These could be used for the ESM. The aim can be simply to optimize the nowcast curves so that they approach the Pareto front. Another aim could be to make the ESM more well-behaved. In a practical implementation, the choice of constant K is based on the intended LX and AEP loss as given by the ground truth Pareto front. Without prior knowledge, there is no guarantee that this tuple of values can be achieved. Here it is argued that, from an operator perspective, it is advantageous if one value of the tuple is preserved. For example, the operator wants to be certain that a particular LX is achieved accepting a higher AEP loss, or, vice versa, the operator defines a particular AEP loss hoping for the best possible LX. A value of K with a completely unpredictable {AEP loss, LX} tuple seems undesirable.

In Section 3.1 just one ensemble member of the nowcast is used. Here, all 20 ensemble members are analyzed by considering the four operators min, max, mean and the median, that are applied to the ensemble vector. It is worth noting that the median operator will indicate rain when more than half of the ensembles indicate rain. Hence, it is equal to utilizing the ESM when the rain probability is above 50 %.
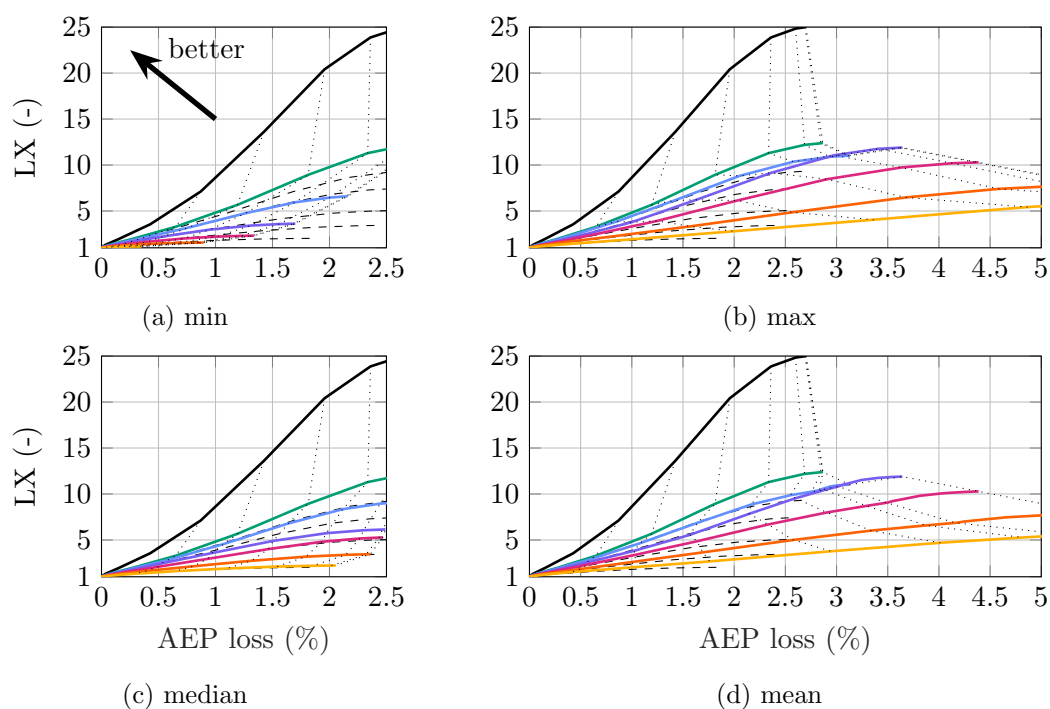

Figure 4: Multi-ensemble results (Lifetime extension factor versus AEP loss) for the VI-ESM; only the De Kooy (#235) site was considered; Pareto front with perfect ground truth precipitation data: ——; Curves obtained using nowcast of 0-min: ——, 5-min: ——, 15-min: ——, 30-min: ——, 60-min: ——, 120-min: ——; single-ensemble VI-ESM curves from Figure 3d for reference: - - -; lines that connect equal K values across curves: ·······.

Figure 4 shows the results of the multi-ensemble nowcast. The results for the 0-minute nowcast are equal for all ensembles, as this is still the latest observation. Hence, the 0-minute results are also equal to the ones from Figure 3d. The curves of the max and mean operator perform almost identically, which is likely a result of the skewness of the ensemble members. It appears that a considerable amount of ensemble members indicate either no rainfall or considerable rainfall. It can be seen that in comparison to the single-ensemble VI-ESM (- - -) the curves for the max and mean operator are moved closer to the Pareto front. This is especially true for the 15-minute nowcast. The higher lead time nowcasts can also achieve a significantly higher LX, albeit at the cost of a high AEP loss. The min operator performs poorly. It can also be seen that the end points of the curves are shifted towards lower AEP losses. This comes at a penalty in LX. Overall, the curves of all lead times are moved into a less favorable direction. The median operator performs similarly in comparison to the single-ensemble nowcast. The 15-minute curve, however, is shifted down.

Table 2: Contingency table for the De Kooy (#235) station with different operators applied to the multi-ensemble nowcast; headers and other information are analogue to Table 1.

	Nowcast	FP	FN	TP	TN	HR	FPR	H_{now}	H_{true}
	perfect	0.00	0.00	7.50	92.49	100.00	0.00	727	727
max	5-min	2.31	0.86	6.62	90.21	88.53	2.50	815	629
max	15-min	4.23	0.77	6.71	88.29	89.69	4.57	1057	628
max	120-min	17.09	1.26	6.26	75.39	83.29	18.48	1810	624
min	5-min	0.60	2.09	5.39	91.92	72.06	0.65	271	629
min	15-min	0.25	3.25	4.24	92.27	56.60	0.27	174	628
min	120-min	0.10	6.81	0.70	92.39	9.34	0.11	15	624
mean	5-min	2.31	0.86	6.62	90.21	88.53	2.50	475	629
mean	15-min	4.23	0.77	6.71	88.29	89.69	4.57	467	628
mean	120-min	17.09	1.26	6.26	75.39	83.29	18.48	336	624
median	5-min	1.23	1.31	6.17	91.29	82.48	1.33	459	629
median	15-min	1.27	1.64	5.85	91.24	78.14	1.38	423	628
median	120-min	1.79	3.89	3.62	90.70	48.21	1.93	196	624

Figure 4 also indicates iso-lines (⋯⋯) that connect data points for the same values of K across the Pareto front and the nowcasting curves. The iso-lines of the median operator run almost straight down from the Pareto front to the 0-minute curve. From that point, they only slightly start deviating up to the 60-minute curve. The iso-lines of the mean operator are almost vertical up to the 15-minute curve. For a starting AEP loss of about 1.25 %, the curve then starts to deviate to the left, whereas for the iso-line starting slightly above 2.25 % the lines quickly deviate to the right. It can be said that the mean and median operators allow for the realization of an ESM that can preserve the indicated AEP loss (when the maximum lead time stays less or equal to 30 minutes) but will yield a variable lifetime. The iso-lines of the max operator move sideways, starting from the 0-minute curve. Hence, with this strategy, one has a high certainty about the LX at the penalty of the variable AEP loss. However, since the iso-line first runs straight down from the Pareto front to the 0-minute curve, the max operator suffers from the problem that an initial estimate for the reduction in the lifetime is required.

In Table 2, it can be seen that the max operator leads to low FN but increases the FP in comparison to the values in Table 1. It is worth noting that the values for FP to TN are equal to the mean operator. A consequence of the fact that both operators will indicate rain when

only one single ensemble indicates $I > 0$ mm/h. Differences can be seen in the predicted rain accumulation. In comparison to the max, the min operator shows the opposite behavior. Max and min constitute boundaries for FN and FP, respectively. It should not be possible to achieve lower values (with straightforward methods). The median operator and single-ensemble values are close. However, the latter has slightly better FN values. From the table, it appears that balanced FP and FN values lead to vertical iso-lines, whereas high values for FP shift the iso-lines to the right. Vice-versa, high FN shift iso-lines to the left. To conclude, the min operator is not a good strategy, due to the underestimating tendency of the nowcasting ensemble. Depending on the goal of the turbine owner the median, mean or max operator could be an appropriate choice.

4. Conclusions

The results showed that a state-of-the-art nowcasting system can be used to drive an ESM and achieve meaningful lifetime gains with limited AEP loss. The 5-minute and 15-minute lead times of the nowcasts provide sufficient accuracy with enough response time to change the speed of the turbine. However, the nowcast-controlled ESM still operates far from the Pareto front. With the current state-of-the-art, achieving a lifetime increase of a factor of five for a penalty of about 1% in AEP seems possible. Depending on the AEP losses caused either by erosion and imperfect repairs or by applying leading-edge protection systems, this may be a worthwhile strategy to mitigate rain erosion damage. The results also showed that the VI-ESM significantly outperforms the traditional V-ESM. Hence, even though the VI-ESM requires a forecast of the rain intensity, it should always be the preferred strategy. The probabilistic information in the multi-ensemble nowcast can be used to improve either the performance or predictability of the ESM. This study also demonstrated that improvements to the skillfulness of nowcasts can drastically improve the viability of the ESM.

References
[1] Bech J I, Hasager C B and Bak C 2018 *Wind Energy Science* **3** 729–748
[2] Barfknecht N, Kreuseler M, de Tavernier D and von Terzi D 2022 *J. Physics: Conf. Series* **2265** 032009
[3] Lin C, Vasić S, Kilambi A, Turner B and Zawadzki I 2005 *Geophysical Research Letters* **32**
[4] Tilg A M, Hasager C B, Kirtzel H J and Hummelshøj P 2020 *Wind Energy Science* **5** 977–981
[5] Overeem A, Uijlenhoet R and Leijnse H 2020 *Journal of Atmospheric and Oceanic Technology* **37** 1643–1660
[6] KNMI 2023 Precipitation - 5 minute precipitation accumulations from climatological gauge-adjusted radar dataset for The Netherlands (1 km) in KNMI HDF5 format Website accessed 01.09.2023 `https://dataplatform.knmi.nl/dataset/rad-nl25-rac-mfbs-5min-2-0`
[7] Imhoff R O *et al.* 2020 *Water Resources Research* **56** e2019WR026723
[8] KNMI 2023 Precipitation - radar/gauge 5-minute ensemble nowcast of precipitation over the Netherlands Website accessed 01.09.2023 `https://dataplatform.knmi.nl/dataset/precipitation-nl-ensemble-nowcast-5min-1-0`
[9] Pulkkinen S *et al.* 2019 *Geoscientific Model Development* **12** 4185–4219
[10] Imhoff R O *et al.* 2021 *Hydrology and Earth System Sciences* **25** 4061–4080
[11] Gaertner E *et al.* 2020 Definition of the IEA 15-megawatt offshore reference wind turbine Tech. rep. NREL, Golden, CO (United States)
[12] DOWA 2020 10 year average wind speed (f) and Weibull scale (a) and shape parameter (k) for height 150m Website accessed 02.01.2024 `https://www.dutchoffshorewindatlas.nl/atlas/image-library/image-library/parameters-per-height-150m`
[13] Verma A S *et al.* 2021 *Wind Energy* **24** 1315–1336
[14] Barfknecht N and von Terzi D 2024 *Wind Energy Science Discussions* **2024** 1–49
[15] Barfknecht N and von Terzi D 2023 *Wind Energy Science Discussions* **2023** 1–42
[16] Bech J I *et al.* 2022 *Renewable Energy* **197** 776–789